



# Probing the structure of Copper(II)-Casiopeina type coordination complexes $[\text{Cu}(\text{O}-\text{O})(\text{N}-\text{N})]^+$ by EPR and ENDOR spectroscopy

Andrea Folli\*, Nadine Ritterskamp, Emma Richards, James A. Platts, Damien M. Murphy\*

School of Chemistry, Cardiff University, Park Place, Cardiff CF10 3AT, UK



## ARTICLE INFO

### Article history:

Received 31 May 2020

Revised 15 July 2020

Accepted 17 July 2020

Available online 28 July 2020

### Keywords:

EPR  
ENDOR  
Copper  
Casiopeina  
Metal complexes

## ABSTRACT

Although copper based complexes have been widely used in homogeneous catalysis, more recently they are attracting considerable attention as pharmaceutical therapeutic agents. Of paramount importance in their efficacy of use is their structure and electronic properties, which can be thoroughly probed using advanced EPR techniques. In this study, a series of  $[\text{Cu}(\text{acac})(\text{N}-\text{N})]^+$  Casiopeina type complexes were investigated, bearing a series of diimine N-N ligands (including bipy, phen, Py-bipy and dppz). All complexes displayed rhombic  $\mathbf{g}$  and  $^{63}\text{A}$  tensors, although the extent of rhombicity was dependent on the N-N ligand. Greater Cu(II)-N2 in-plane distortion, away from the square planar arrangement, was detected by CW W-band EPR for the smaller bipy and phen ligands compared to the larger Py-bipy and dppz ligands. Changes in ligand spin density distributions (over the  $^1\text{H}$  and  $^{14}\text{N}$  nuclei) were revealed by CW Q-band ENDOR. The largest components of the  $^1\text{H}$  imine and  $^{14}\text{N}$  hyperfine coupling decreased as the ligand size increased, following the trend bipy > phen > Py-bipy > dppz. These results indicate how even small structural and electronic (spin density) perturbations within the Casiopeina family of Cu(II) complexes can be probed by advanced EPR methods.

© 2020 The Author(s). Published by Elsevier Inc. This is an open access article under the CC BY license (<http://creativecommons.org/licenses/by/4.0/>).

## 1. Introduction

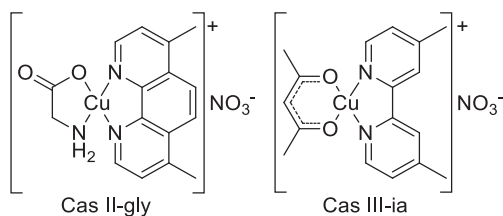
The Casiopeinas are a class of mixed chelate, cationic copper complexes which have well known antineoplastic properties. They have the general formula  $[\text{Cu}(\text{O}-\text{O})(\text{N}-\text{O})]^+$  or  $[\text{Cu}(\text{O}-\text{O})(\text{N}-\text{N})]^+$ , where O-O typically represents an acetylacetonate (abbreviated to acac) or salicylaldehyde (sal) chelate ligand, N-O denotes an aminoacidate or peptide, and N-N generally indicates an aromatic diimine such as 1,10-phenanthroline (phen) or 2,2'-bipyridine (bipy) [1]. The most commonly studied derivatives are based on the  $[\text{Cu}(4,7\text{-dimethyl-1,10-phenanthroline})(\text{glycinato})]\text{NO}_3$  complex [2–5] (labelled Cas II-gly) and the  $[\text{Cu}(4,4'\text{-dimethyl-2,2'-bipyridine})(\text{acetylacetonato})]\text{NO}_3$  complex [2,3,6,7] (labelled Cas III-ia), see Scheme 1. These complexes and numerous analogues [8–12] have been evaluated both *in vitro* and *in vivo*, and have demonstrated antineoplastic [13], cytotoxic [14], genotoxic [2,12] and antiviral activities. Whilst some Casiopeinas have been found to be active on cisplatin-resistant cell lines [4,15], a considerable amount of work is still required before they can be used in a clinical setting [16]. Nevertheless, their potential to combat a broader spectrum of disease with fewer toxic side effects has stimulated

extensive studies on the characterisation of this class of complex.

Whilst Cu(I/II) systems bearing O-O, N-O and N-N ligands have been routinely employed in a vast array of heterogeneous and homogeneous reactions, including aerobic alcohol oxidation [17–19], water oxidation catalysis [20–22], and in challenging C-C/C-N bond coupling [23–25], the full catalytic utility of the  $[\text{Cu}(\text{O}-\text{O})(\text{N}-\text{O})]^+$  class of complexes has never been thoroughly explored. Whether employed as catalysts or therapeutic agents, understanding the structure and detailed electronic properties of such complexes is crucial to explaining their activity. Even their mode of action as therapeutic agents, for which these complexes are best known, remains poorly understood. DNA has been established as its primary cellular target and the planar aromatic diimine ligand is suggested to bind DNA by intercalative [26–29] and non-intercalative interactions [30]. Once bound, the redox properties of the copper centre are capable of generating reactive oxygen species (ROS) which can cause oxidative damage to the DNA, postulated to ultimately result in cell death [30–35]. Adduct formation between the copper complex and the DNA may induce conformational change within a strand of DNA and cause denaturation. This could also contribute to the therapeutic mechanism of Casiopeinas. It has been demonstrated that cisplatin acts by forming inter-strand crosslinks between guanine bases causing the DNA to kink, preventing replication processes [34–36].

\* Corresponding authors.

E-mail addresses: [FolliA@cardiff.ac.uk](mailto:FolliA@cardiff.ac.uk) (A. Folli), [MurphyDM@cardiff.ac.uk](mailto:MurphyDM@cardiff.ac.uk) (D.M. Murphy).



**Scheme 1.** Structures of Cas II-gly and Cas III-ia Casiopeina complexes.

Quantitative structure-activity relationship (QSAR) studies indicate that the biological activities of Casiopeina type anticancer agents are affected by substitution effects on the ligands [2]. For instance, electron donating ligands on the diimine ligand were found to increase anti-tumour activity by modulating the redox chemistry of the copper centre [2]. In contrast, electron withdrawing groups present on the diimine ligand increased the stability of intercalative  $\pi$ - $\pi$  interactions between the diimine and nucleobases of the DNA scaffold [29]. In addition, phen-type derivatives have been found to be more active than their bipy-type counterparts, suggesting that the size of the aromatic ring system of the diimine ligand influences the DNA affinity for the copper complex. Clearly, there is a delicate balance to achieve in order to optimise the performance of these complexes.

A complete description of the electronic and geometric structure of the Casiopeina type complexes in both the ‘unbound’ state (free of DNA) and in the bound DNA adduct, may therefore offer interesting insights into the therapeutic action of this class of compounds and ultimately contribute to the design of novel casiopeina inspired drugs with improved therapeutic activity. Electron Paramagnetic Resonance (EPR) and its related hyperfine techniques, such as Electron Nuclear Double Resonance (ENDOR), can offer an unprecedented measure of this electronic and geometric information, as has in the past been demonstrated for the elucidation of the structure-function relationships in copper proteins [37–39], and thus these methods have the potential to examine and interrogate the structure of these copper based therapeutics in exquisite detail. A small number of papers have used EPR to study the covalency in the Casiopeina complexes [7], whilst Chikira *et al.*, [26,40] focussed on the  $g$  and  $^{\text{Cu}}A$  parameters when the copper complexes were intercalatively bound to DNA fibres. By comparison, no ENDOR or multi-frequency EPR studies of these complexes have been reported. Unlike EPR, ENDOR is able to probe the configuration of surrounding spin-active ligand nuclei, providing more detailed information on the overall electronic structure of the complex. Indeed the importance of electron distribution in these complexes was highlighted in an experimental and theoretical study by Ruiz-Azuara *et al.* [41]. This level of detail in the electronic structure may be necessary in order to resolve subtle structural differences in the complexes which may have significant consequences in terms of activity.

In this work, we have therefore prepared a series of unbound Casiopeina complexes with the general formula  $[\text{Cu}(\text{acac})(\text{N-N})]^+$  and thoroughly explored their electronic properties through the spin Hamiltonian parameters using EPR and ENDOR spectroscopy combined with DFT calculations. Within the series of complexes studied, the diimine ligand (N-N) was systematically varied in size using 2,2'-bipyridine (bipy), 1,10-phenanthroline (phen), a pyridine substituted 2,2'-bipyridine ligand (Py-bipy) and dipyrindophenazine (dppz); Scheme 2. These diimine ligands were selected due to the fact that the size of the aromatic diimine ligand may influence the therapeutic activity.

## 2. Experimental section

### 2.1. Materials

The copper salt  $\text{Cu}(\text{CF}_3\text{SO}_3)_2$  used throughout this study was sourced from Sigma Aldrich. Acetylacetonate and the diimine ligands 2,2'-bipyridyl (bipy), 1,10-phenanthroline (phen) and 2,3-bis(2-pyridyl)pyrazine (Py-bipy) were also bought from Sigma Aldrich and used as received. Reagent grade ethanol (EtOH) and dimethylformamide (DMF) were purchased from Sigma Aldrich and used without further purification. Deuterated solvents, EtOD- $d_6$  and DMF- $d_7$ , were sourced from Goss Scientific in sealed ampules and used as received.

### 2.2. Sample preparation

Complexes with the general formula of  $[\text{Cu}(\text{acac})(\text{N-N})]^+$  were prepared using methods described in the literature [42]. Once isolated and purified, 0.03 M solutions of the  $[\text{Cu}(\text{acac})(\text{N-N})]^+$  complexes were prepared in an EtOH:DMF (1:1) solvent system and flash frozen to 140 K for X-band EPR analysis. Q-band EPR,  $^1\text{H}$  and  $^{14}\text{N}$  ENDOR studies were performed using 0.03 M solutions prepared in EtOD- $d_6$ :DMF- $d_7$  (1:1) at 10 K. The same solvent system were used for W-band EPR studies with a sample preparation of 0.04 M.

### 2.3. EPR/ENDOR spectroscopy

The continuous wave (CW) X-band (9.5 GHz) EPR measurements were performed on a Bruker EMX spectrometer utilizing an ER4119HS resonator, 100 kHz field modulation at 140 K or 298 K and typically using 10.17 mW MW power. The CW Q-band (35 GHz) EPR and ENDOR measurements were recorded on a Bruker Elexsys E500 spectrometer using a Bruker ER5106 QT-E Q-band resonator operating at 10 kHz field modulation and 10 K for ENDOR (and at 100 kHz and 50 K for the EPR). The CW Q-band ENDOR spectra were obtained using 1 dB RF power from an ENI 3200L RF amplifier at 100 kHz RF modulation depth and 0.5 mW microwave power. The CW W-band (95 GHz) EPR measurements were performed on a Bruker Elexsys E600 spectrometer using a Bruker E600-1021H TeraFlex resonator operating at 100 kHz field modulation frequency, 7 G field modulation amplitude and 20 K, using 1.58  $\mu\text{W}$  MW power.

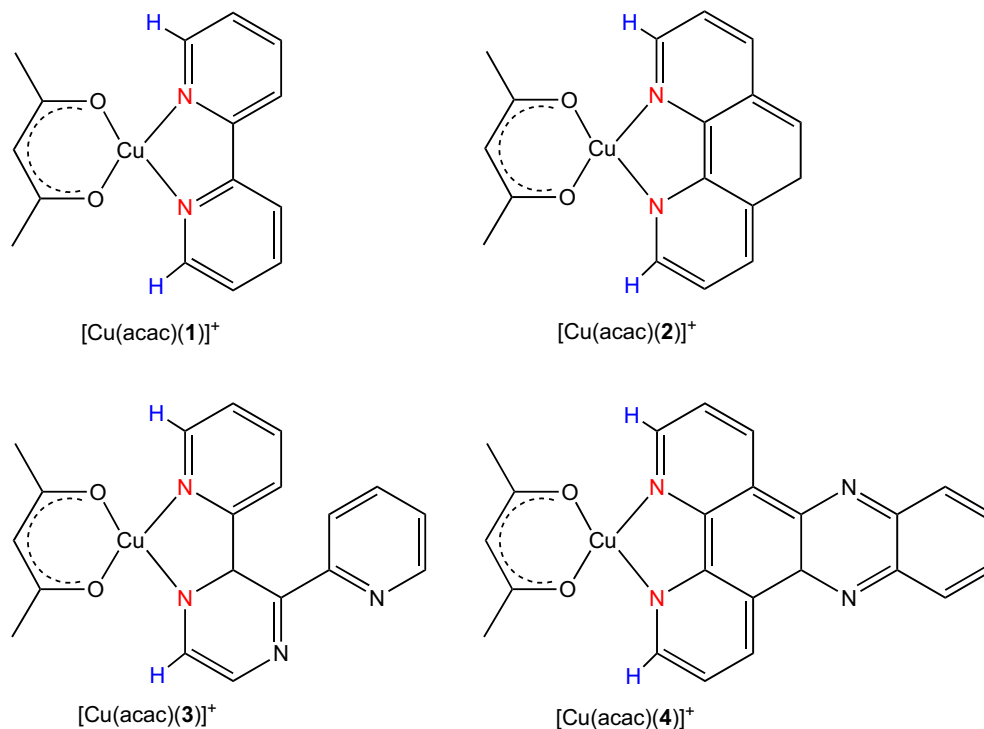
All DFT calculations used the OCRA package. The complexes  $[\text{Cu}(\text{acac})(\mathbf{1-4})]^+$  were geometry optimized at the M06-2X/def2TZVP level. EPR parameters were predicted using the PBE0 functional and a basis set consisting of EPR-II on light atoms and the ‘‘core properties’’ set on copper [43–46].

EPR and ENDOR simulations were performed using the Easyspin [47] software package running within the MathWorks<sup>®</sup> MatLab<sup>®</sup> environment.

## 3. Results and discussion

### 3.1. CW X-, Q- and W-band EPR.

The experimental and simulated CW X-band EPR spectra (recorded at 140 K) of the four Casiopeina type complexes  $[\text{Cu}(\text{acac})(\mathbf{1-4})]^+$  dissolved in EtOH:DMF are shown in Fig. 1. At this frequency (X-band), the superhyperfine couplings from remote nuclei are clearly visible and, owing to the relatively small  $g_3$  ( $g_{\parallel}$ ) values expected of the largely square planar copper complexes, a pronounced overshoot feature dominates all spectra. These X-band EPR spectra (Fig. 1) are similar to analogous Cu(II) complexes possessing a largely square planar geometry [48] with quasi axial



**Scheme 2.** Structures of the Casiopeina type complexes of general formula [Cu(acac)(N-N)]<sup>+</sup>, where N-N represents 2,2'-bipyridine (bipy) [Cu(acac)(1)]<sup>+</sup>, 1,10-phenanthroline (phen) [Cu(acac)(2)]<sup>+</sup>, the pyridine substituted 2,2'-bipyridine (Py-bipy) [Cu(acac)(3)]<sup>+</sup> and dipyriddyphenazine (dppz) [Cu(acac)(4)]<sup>+</sup>; the CF<sub>3</sub>SO<sub>3</sub> anion (OTf) was used in all cases.

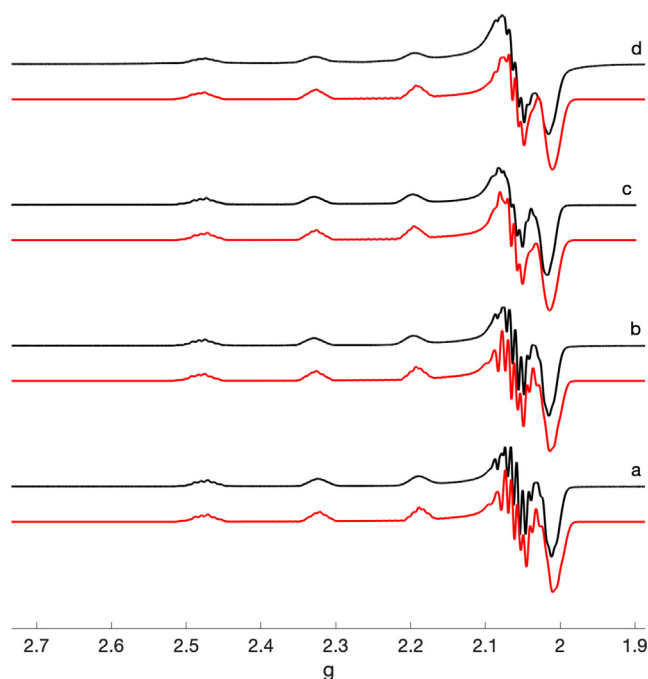


**Fig. 1.** CW X-band EPR spectra (recorded at 140 K) of a) [Cu(acac)(1)]<sup>+</sup>, b) [Cu(acac)(2)]<sup>+</sup>, c) [Cu(acac)(3)]<sup>+</sup> and d) [Cu(acac)(4)]<sup>+</sup>, using OTf counterions in all cases. All complexes were dissolved in EtOH:DMF (1:1) and recorded as frozen solutions. The corresponding simulations are shown by the red traces.

symmetry. The <sup>14</sup>N superhyperfine splitting, caused by the two nitrogen nuclei (<sup>14</sup>N, *I* = 1) of the diamine ligand, are clearly visible (Fig. 1), both at the low  $g = g_{\parallel}$  field ( $m_l = +3/2$ ) and at higher  $g = g_{\perp}$

field positions. However, the contributions to the spin Hamiltonian parameters from the two <sup>63,65</sup>Cu isotopes and the <sup>14</sup>N nuclei cannot be confidently determined from the X-band EPR spectra alone.

In general, large <sup>14</sup>N superhyperfine couplings can be directly observed in the X-band spectra of Cu(II) nitrogen macrocycles [49–56]. However, as the *g*-anisotropy is responsible for the overlap of the  $g_1$ ,  $g_2$  and  $g_3$  features, accurate determination of the *g*-values due to the superimposed <sup>14</sup>N superhyperfine pattern requires measurement at higher microwave frequencies. Higher frequency EPR measurements were therefore recorded for all four complexes. The resulting illustrative measurements at Q- and W-band frequencies for [Cu(acac)(1)]<sup>+</sup> are shown in Fig. 2 (the corresponding spectra for the three remaining complexes [Cu(acac)(2–4)]<sup>+</sup> are shown in Fig.S1 of the Supporting Information). The simulated spin Hamiltonian parameters, extracted by analysis of the multi-frequency EPR spectra for all four complexes, are listed in Table 1. The <sup>14</sup>N (and large imine <sup>1</sup>H) couplings responsible for the prevailing superhyperfine pattern in the X-band EPR spectra (Fig. 1), were extracted from the simulated ENDOR spectra (*vide infra*) and, combined with the accurate *g* and <sup>63</sup>Cu values, used to generate the resulting X-band EPR simulations.

The W-band spectra are particularly sensitive and informative in revealing subtle differences in the *g* values for all four complexes. A stack plot of the measured W-band spectra is reported in Fig. 3 to exemplify this. Interestingly, simulation of the experimental spectra (Table 1) revealed that all of the complexes show a small degree of rhombicity in their *g* tensor (rhombic symmetry with  $g_x \neq g_y \neq g_z$  whilst the *g* and *A* frames are coincident), not resolved at X- or Q-band; however, the rhombicity appears to decrease with increasing diimine ligand size (column  $\Delta g_{yx}$  in Table 1). The magnitude of this experimentally detected rhombic distortion was quite subtle, and notably not detected in the DFT analysis, which did not reveal this trend. Furthermore, the measurements were recorded with different ratios of solvent (EtOH:

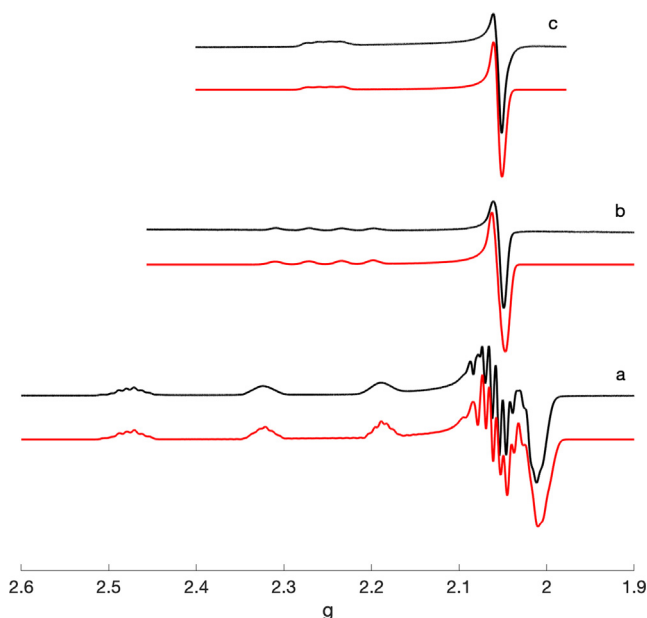


**Fig. 2.** Multi-frequency CW EPR spectra of 2,2'-bipyridine (bipy)  $[\text{Cu}(\text{acac})(\mathbf{1})]^+$  ( $\mathbf{1}$  = 2,2'-bipyridine) recorded at a) X-, b) Q- and c) W-band frequencies. All complexes were recorded as frozen solutions after dissolution in EtOH:DMF (1:1).

DMF) and after freezing under slightly different conditions; in all cases the distortion was experimentally detected, so unlikely to be due to incomplete orientational averaging in the frozen solution. These observations may suggest a slightly greater degree of distortion or twisting in the  $\text{Cu}(\text{II})\text{-N}_2$  plane for the bipy and phen based complexes  $[\text{Cu}(\text{acac})(\mathbf{1}\text{--}\mathbf{2})]^+$  compared to the Py-bipy and dppz based complexes  $[\text{Cu}(\text{acac})(\mathbf{3}\text{--}\mathbf{4})]^+$ , enabling the  $\text{Cu}(\text{II})$  ion to retain a more localised axial environment in the latter two complexes. This small distortion away from square planar geometry could not be detected in the DFT optimised structures.

### 3.2. $^1\text{H}$ ENDOR

At the higher microwave frequencies, the  $^{14}\text{N}$  and imino  $^1\text{H}$  superhyperfine splitting is lost in the CW EPR spectra due to significant strain effects. To successfully extract the superhyperfine couplings, and in the specific case of  $^{14}\text{N}$ , the additional quadrupole coupling, angular selective  $^1\text{H}$  and  $^{14}\text{N}$  ENDOR measurements were performed. ENDOR spectroscopy provides far more information on the extent of spin delocalisation onto the surrounding ligand [57–62], which is an important factor when considering the possible intercalation ability of these complexes [27]. A set of Q-band CW

angular selective  $^1\text{H}$  ENDOR spectra are shown in Fig. 4 for the case of  $[\text{Cu}(\text{acac})(\mathbf{1})]^+$ . The hyperfine parameters extracted from the associated simulations of the imino protons exclusively are listed in Table 2, in order to compare with the DFT derived values. Comparison between the  $^1\text{H}$  ENDOR spectra of the four complexes at one fixed field position is reported in Fig. 5. All four complexes produce an analogous and generic  $^1\text{H}$  ENDOR pattern, which are dominated by the large coupling arising from the imine  $^1\text{H}$  (labelled blue in Scheme 2). For this reason, only the ENDOR spectra of  $[\text{Cu}(\text{acac})(\mathbf{1})]^+$  will be described in detail here, whilst the necessary comparisons for the other three  $[\text{Cu}(\text{acac})(\text{N-N})]^+$  complexes (Table 2) will be discussed accordingly.

A distinct feature for all these copper complexes is the large coupling arising from the imine protons, as reported elsewhere in the literature for salen and oxime based copper complexes [50,53,54–56]. This large coupling can be attributed to the considerable conjugation of the imine proton with the coordinating nitrogen atoms, resulting in significant unpaired spin density delocalising over the proton. The maximum coupling for the two imino  $^1\text{H}$  in  $[\text{Cu}(\text{acac})(\mathbf{1})]^+$  is observed at the field position corresponding to  $g = 2.054 \cong g_x \approx g_y$ , (i.e.  $g_{\perp}$ ) with a value of 10.25 MHz. This is in good agreement with the relative orientation of the **A** tensor frame with respect to the **g** tensor frame, as seen in Fig. 6. The very small difference in coupling, and hence spin density on the proton, between the complexes studied herein is evident from the experimental ENDOR spectra (Fig. 5). These spectra provide direct experimental evidence for the small variation in spin densities depending on the nature of the diamine backbone. It should be noted that only the large imine proton couplings are included in the simulation shown in Fig. 4. The remaining smaller proton couplings arising from the acetylacetonato ligand (responsible for the inner peaks in Fig. 4) were not included. A detailed description of these latter methine and methyl proton couplings for  $[\text{Cu}(\text{acac})_2]$  was reported elsewhere by us [63], including the couplings from the complete averaging of the rotating methyl group protons and those from a subset of methyl group protons undergoing hindered rotation on the EPR time scale producing a pronounced anisotropic hyperfine tensor. As these couplings are very solvent dependent, they were not included in the current simulations.

In the **A** tensor coordinates, the largest hyperfine coupling value lies on the z axis (Table 2), which align with the x-y plane of the **g** tensor, and which is also the molecular plane. The imino  $^1\text{H}$  **A** tensor exhibits quasi axial symmetry, with the two remaining hyperfine components (indistinguishable within the experimental errors, Table 2) equal to 2.6 MHz and 2.8 MHz, oriented above and below the molecular plane. The isotropic hyperfine value of 5.22 MHz is notably smaller when compared to the  $^1\text{H}$ -imine couplings reported for Cu-salen ( $a_{\text{iso}} = 19.26$  MHz) [48,51] and Cu-oxime ( $a_{\text{iso}} = 10.21$  MHz) [55,56] type complexes, due to the considerable

**Table 1**

Experimental and DFT derived spin Hamiltonian **g** and  $^{\text{Cu}}\mathbf{A}$  principal values (i.e. in the **g** and  $^{\text{Cu}}\mathbf{A}$  frame coordinates respectively) for the  $[\text{Cu}(\text{acac})(\text{N-N})]\text{OTf}$  complexes ( $\mathbf{1}\text{--}\mathbf{4}$ ).

Compound		$g_x$	$g_y$	$\Delta g_{yx}$	$g_z$	$g_{\text{iso}}$	$^{\text{Cu}}A_x$	$^{\text{Cu}}A_y$	$^{\text{Cu}}A_z$	$^{\text{Cu}}a_{\text{iso}}$
							/MHz	/MHz	/MHz	/MHz
<b>1</b>	exp	2.050	2.057	0.007	2.253	2.120	−46	−46	−551	−214
	DFT	2.043	2.046	0.003	2.148	2.0788	−127	−129	−857	−371
<b>2</b>	exp	2.054	2.060	0.006	2.259	2.124	−46	−46	−551	−214
	DFT	2.043	2.046	0.003	2.151	2.0802	−128	−131	−858	−372
<b>3</b>	exp	2.055	2.059	0.004	2.258	2.124	−35	−35	−541	−204
	DFT	2.042	2.046	0.004	2.149	2.0791	−123	−131	−852	−369
<b>4</b>	exp	2.055	2.057	0.002	2.257	2.123	−35	−35	−551	−207
	DFT	2.043	2.047	0.004	2.154	2.0813	−127	−130	−859	−372

Note: The **g** and  $^{\text{Cu}}\mathbf{A}$  tensor frames are mostly collinear and rotated from the arbitrary molecular frame coordinates according to the following Euler angles (in radians) using the 'zyz' convention:  $\alpha = -\pi/2, \beta = 0, \gamma = 0$  (bipy);  $\alpha = \pi/2, \beta = 0, \gamma = 0$  (phen);  $\alpha = -1, \beta = \pi, \gamma = 2$  (Py-bipy);  $\alpha = -1, \beta = \pi, \gamma = 2$  (dppz). Uncertainty on the **g** values is  $\pm 0.002$ , and on the **A** values is  $\pm$  ca. 2 MHz for  $A_x$  and  $A_y$  and  $\pm$  ca. 6 MHz for  $A_z$ .

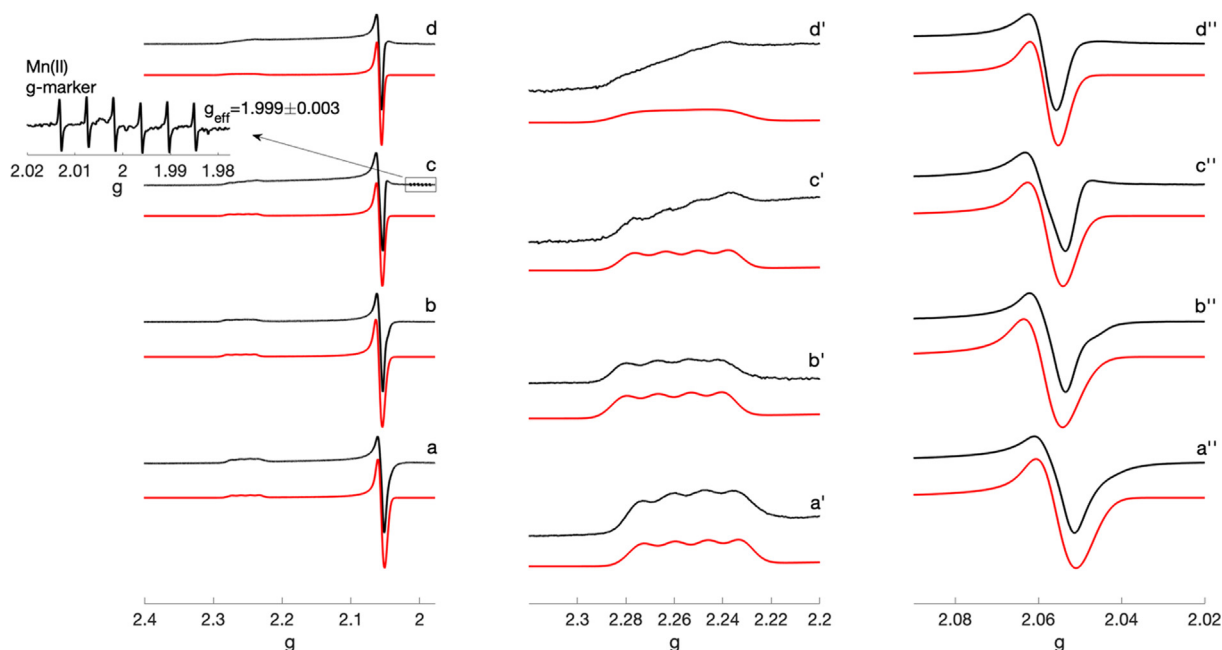


**Fig. 3.** W-band CW EPR spectra (recorded at 20 K) of a-a'-a'' [Cu(acac)(1)]<sup>+</sup>, b-b'-b'' [Cu(acac)(2)]<sup>+</sup>, c-c'-c'' [Cu(acac)(3)]<sup>+</sup> and d-d'-d'' [Cu(acac)(4)]<sup>+</sup>, using a OTf counterions in all cases. All complexes dissolved in EtOH:DMF (1:1). Corresponding simulations are shown in red traces. a-d) shows the wide sweep; a'-d') narrow sweep highlighting the  $g \sim g_{\parallel}$  region and a''-d'') narrow sweep highlighting the  $g \sim g_{\perp}$  region. When recording complex [Cu(acac)(3)]<sup>+</sup> a Mn(II) g-marker was also used to calibrate  $g$  values measurements.

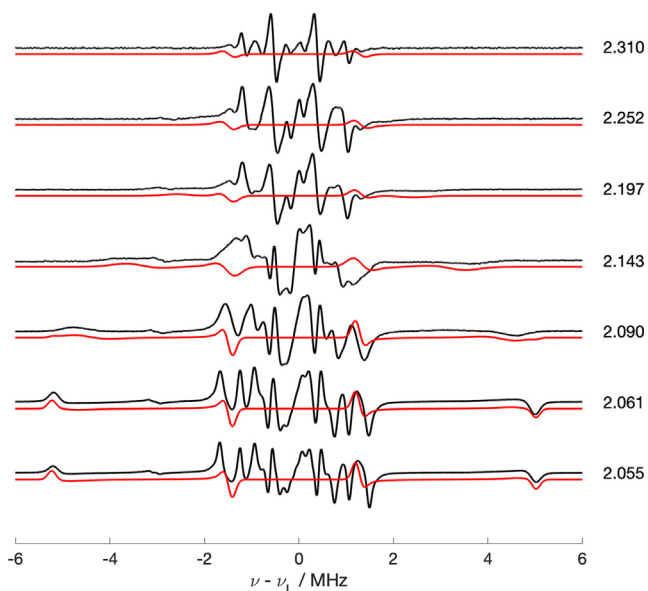


**Fig. 4.** Q-band CW <sup>1</sup>H ENDOR spectra (10 K) of [Cu(acac)(1)]<sup>+</sup> dissolved in EtOH-d<sub>6</sub>:DMF-d<sub>7</sub> (1:1) recorded at the field positions corresponding to the labelled  $g$ -values. The corresponding simulations are shown in red trace.

**Table 2**  
Experimental and DFT derived imino <sup>1</sup>H principal hyperfine values (i.e. in the <sup>1</sup>H $\mathbf{A}$  frame coordinates) for the [Cu(acac)(1)]<sup>+</sup> complex.

Compound		$A_x$	$A_y$	$A_z$	$a_{iso}$	$\alpha$	$\beta$	$\gamma$
		/MHz	/MHz	/MHz	/MHz	/rad	/rad	/rad
<b>1</b>	H8 exp	2.6	2.8	10.25	5.22	0.30	$\pi/2$	$\pi/4$
	H8 DFT	3.1	4.6	11.3	6.33	0.31	$\pi/2$	0.63
	H12 exp	2.6	2.8	10.25	5.22	-0.30	$\pi/2$	$-\pi/4$
	H12 DFT	3.1	4.6	11.3	6.33	-0.33	$\pi/2$	-2.74

Note: The provided Euler angles are associated with the rotation that transforms the molecular frame to the  $\mathbf{A}$  tensor frame. Uncertainty in the  $A$  values is  $\pm 0.2$  MHz for  $A_x$  and  $A_y$  and  $\pm 0.5$  MHz for  $A_z$ . Uncertainty on the Euler angles is  $\pm 0.2$  rad.

reduction in ligand based unpaired spin density. Overall the <sup>1</sup>H imine coupling for the [Cu(acac)(1–4)]<sup>+</sup> complexes possess a positive <sup>1</sup>H tensor with the largest hyperfine components being 10.25 MHz (bipy), 10.00 MHz (phen), 10.25 MHz (Py-bipy) and 9.80 MHz (dppz), respectively, Fig. 5. The decrease in magnitude of the coupling appears to partially correlate with the increase size of the diimine ligands and suggests that the imine proton couplings are very sensitive to the delocalisation of the spin density over the aromatic ring system. The coupling magnitude is greatest for 2,2'-bipyridine, [Cu(acac)(1)]<sup>+</sup>, where the spin density is delocalised over two six-membered rings whilst it is smallest for the dppz ligand, [Cu(acac)(4)]<sup>+</sup>, where the spin density is delocalised over a more extended aromatic ring framework, whilst noting that the more twisted (non planar) Py-bipy system has a slightly larger  $a_{iso}$  value. This trend was not only observed experimentally but, within experimental error, also was predicted by DFT; i.e., 11.27 MHz (bipy), 11.05 MHz (phen), 11.23 MHz (Py-bipy) and 10.98 MHz (dppz).

### 3.3. <sup>14</sup>N ENDOR

The <sup>14</sup>N superhyperfine patterns clearly observed in the CW X-band EPR spectra (Fig. 1) are a rich source of structural information and can potentially help to understand the coordination of the dif-

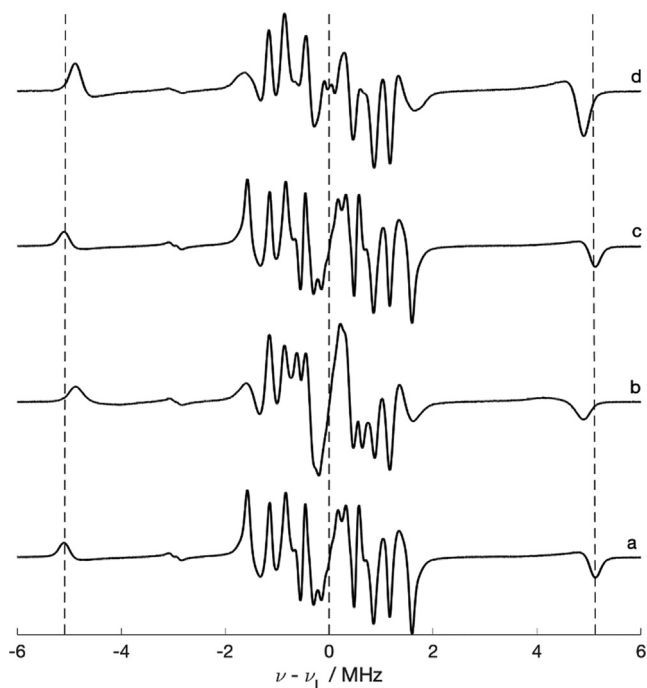


**Fig. 5.** Comparative Q-band CW  $^1\text{H}$  ENDOR spectra (10 K) of a)  $[\text{Cu}(\text{acac})(\mathbf{1})]^+$ , b)  $[\text{Cu}(\text{acac})(\mathbf{2})]^+$ , c)  $[\text{Cu}(\text{acac})(\mathbf{3})]^+$  and d)  $[\text{Cu}(\text{acac})(\mathbf{4})]^+$ , dissolved in  $\text{EtOD-d}_6$ : $\text{DMF-d}_7$  (1:1), recorded at the field positions corresponding to  $g = g_{\perp}$ .

ferent diimine ligands to the copper centre. In order to extract the  $^{14}\text{N}$  hyperfine and nuclear quadrupole values from the diimine ligand, Q-band CW ENDOR measurements were conducted. The experimental and corresponding angular selective  $^{14}\text{N}$  simulations for  $[\text{Cu}(\text{acac})(\mathbf{1})]^+$  are shown in Fig. 7.

The  $^{14}\text{N}$  couplings are well resolved, enabling one to simulate the angular selective profile more accurately compared to using CW EPR alone. The resulting couplings are given in Table 3. Very good agreement was obtained between the experimental and DFT derived values. The hyperfine and quadrupolar coupling from

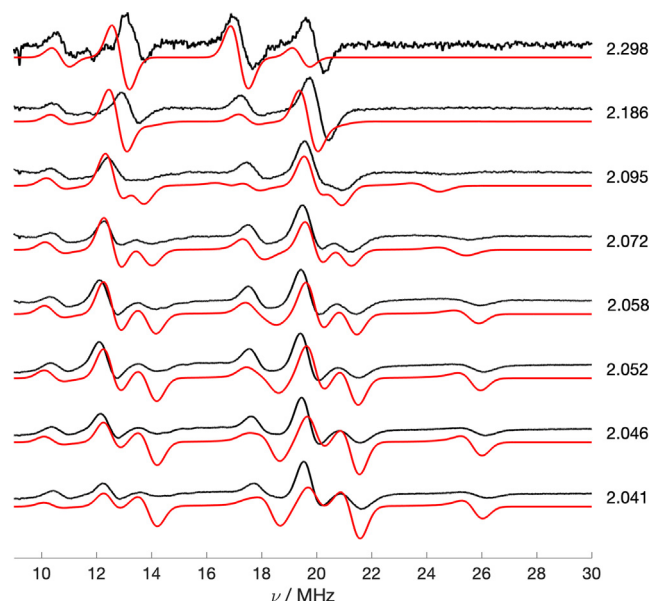


**Fig. 7.** Q-band CW  $^{14}\text{N}$  ENDOR spectra (measured at 10 K) of  $[\text{Cu}(\text{acac})(\mathbf{1})]^+$  dissolved in  $\text{EtOH-d}_6$ : $\text{DMF-d}_7$  (1:1) recorded at the field positions corresponding to the labelled  $g$ -values. Corresponding simulations shown as red trace.

the  $^{14}\text{N}$  ( $I = 1$ ) nuclei appears to have axial symmetry with the largest hyperfine coupling of 40 MHz that aligns with the molecular plane. From the two  $^{14}\text{N}$  nuclei appear equivalent in the experimental spectra. The magnitude of the couplings as is expected for imino complexes of this type. For the  $^{14}\text{N}$  ENDOR measurements, that the size of the diimine ligand has a subtle impact on the magnitude of the hyperfine coupling, in the following order for the largest  $^{14}\text{N}$  coupling of 40.0 MHz (bipy), 39.1 MHz (phen), 39.1 MHz (Py-bipy) and 38.8 MHz (dppz), Fig. 8. This is analogous to the trends observed with the  $^1\text{H}$  data, indicating an overall decrease in  $^{14}\text{N}$  ligand spin densities.

It should be noted that Galindo-Murillo et al., [27] highlighted the importance of  $\pi$ -stacking effects between Casiopeinas and DNA bases. The importance of the aromatic ligand moiety on the

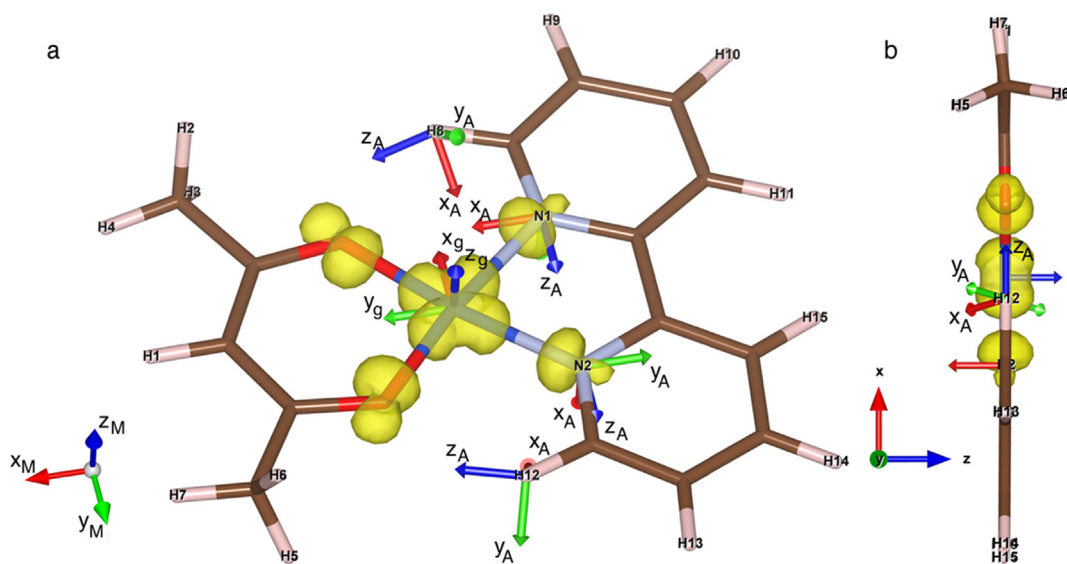


**Fig. 6.** a) Geometry optimized DFT structure of  $[\text{Cu}(\text{acac})(\mathbf{1})]^+$ , showing the relative orientation of the molecular,  $g$ -imino- $^1\text{H}$  and  $^{14}\text{N}$  principal axes. b) View of the complex in a) illustrating the alignment of the imino  $^1\text{H}$   $z_A$  axis with respect to the molecular plane.

**Table 3**  
Experimental and DFT calculated  $^{14}\text{N}$  principal hyperfine and quadrupole values (i.e. in the  $^{14}\text{N}\mathbf{A}$  and  $^{14}\text{N}\mathbf{Q}$  frame coordinates) for the  $[\text{Cu}(\text{acac})(\mathbf{1})]^+$  complex.

Compound		$A_x$	$A_y$	$A_z$	$a_{\text{iso}}$	$\alpha$	$\beta$	$\gamma$	$Q_x$	$Q_y$	$Q_z$	$\alpha$	$\beta$	$\gamma$
		/MHz	/MHz	/MHz	/MHz	/rad	/rad	/rad	/MHz	/MHz	/MHz	/rad	/rad	/rad
<b>1</b>	N1 exp	30	30	40	33.3	$\pi/2$	$\pi/2$	$-\pi/2$	0.75	0.75	-1.5	$\pi/2$	$\pi/2$	$-\pi/2$
	N1 DFT	32	33	43	36	1.44	1.87	-1.67	0.56	0.82	-1.38	1.72	1.28	p
	N2 exp	30	30	40	33.3	$\pi/2$	$\pi/2$	0	0.75	0.75	-10.5	$\pi/2$	$\pi/2$	0
	N2 DFT	32	33	43	36	1.81	1.79	-0.41	0.56	0.82	-1.38	0.36	1.36	-2.90

Note: The provided Euler angles are associated with the rotation that transforms the molecular frame to the  $\mathbf{A}$  tensor frame and  $\mathbf{Q}$  frame respectively. Uncertainty on the  $\mathbf{A}$  values is  $\pm 2$  MHz and on the  $\mathbf{Q}$  values is  $\pm 0.1$  MHz. Uncertainty on the Euler angles is  $\pm 0.2$  rad.

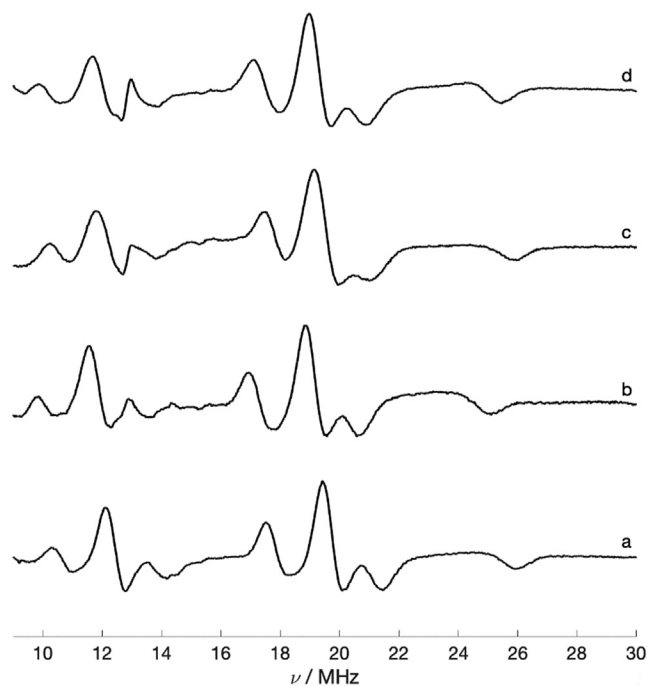


**Fig. 8.** Comparative Q-band CW  $^{14}\text{N}$  ENDOR spectra (10 K) of a)  $[\text{Cu}(\text{acac})(\mathbf{1})]^+$ , b)  $[\text{Cu}(\text{acac})(\mathbf{2})]^+$ , c)  $[\text{Cu}(\text{acac})(\mathbf{3})]^+$  and d)  $[\text{Cu}(\text{acac})(\mathbf{4})]^+$ , dissolved in EtOD- $d_6$ :DMF- $d_7$  (1:1), recorded at the field positions corresponding to  $g = g_{\perp}$ .

DNA intercalation effect was evident, such that the stacking mechanism adopted was shown to depend on the electron density deficiency of the ligands which was compensated by an electron transfer from adenines by a  $\pi$ - $\pi$  interaction [27]. Here, we have shown that the spin density distribution in the complexes is subtly dependent on the nature of the diimine backbone ligand. As the conjugated ring size increases, both the  $^1\text{H}$  and  $^{14}\text{N}$  spin densities decrease accordingly, as may well be expected. However, less obvious to predict is the subtle distortion within the  $\text{Cu}(\text{II})\text{-N}_2$  plane which, according to the W-band EPR measurements, appears to be greater with smaller diimine ligands (bipy and phen) compared to the large ring systems (Py-bipy and dppz). These results indicate how small structural and electronic perturbations to the Casiopeinas family of  $\text{Cu}(\text{II})$  complexes can be interrogated and probed by advanced EPR methods.

#### 4. Conclusions

Casiopeina type copper complexes have been studied for many years, as they show promising potential as therapeutic agents. The therapeutic action of the Casiopeina complexes still remains unclear [16] and many approaches have been made to explore this mechanism, from systematic structural modifications of the com-

plex to detailed spectroscopic studies. To date, very few advanced EPR studies have been conducted on these systems. Therefore, in this study a series of Casiopeina type complexes of general formula  $[\text{Cu}(\text{O}-\text{O})(\text{N}-\text{N})]^+$  were prepared, and their electronic properties examined by EPR and ENDOR spectroscopy. Within this  $[\text{Cu}(\text{acac})(\text{N}-\text{N})]^+$  series, the diimine ligand (N-N) was systematically varied in size using 2,2'-bipyridine (bipy), 1,10-phenanthroline (phen), a pyridine substituted 2,2'-bipyridine ligand (Py-bipy) and dipyrrophenazine (dppz), whilst retaining the acetylacetonato ligand throughout (i.e.,  $[\text{Cu}(\text{acac})(\text{N}-\text{N})]^+$ ). These diimine ligands were selected since it is believed that variation in the aromatic diimine ligand size may influence the therapeutic activity via DNA intercalation effects.

The EPR spectra of these  $[\text{Cu}(\text{acac})(\mathbf{1}-\mathbf{4})]^+$  complexes were all characterised by a slightly rhombic set of  $g$  and  $^{63}\text{Cu}$  values. However, the degree of rhombicity, caused by a small in-plane twisting within the  $\text{Cu}(\text{II})\text{-N}_2$  framework away from the ideal square planar arrangement, was most pronounced for the smaller diimine ligands (in the  $[\text{Cu}(\text{acac})(\mathbf{1}-\mathbf{2})]^+$  complexes) compared to the larger ligands (in the  $[\text{Cu}(\text{acac})(\mathbf{3}-\mathbf{4})]^+$  complexes). This variation in EPR parameters as a function of N-N ring size was also matched by considering the observed changes in the isotropic  $^{63}\text{Cu}$  values, which were largest for  $[\text{Cu}(\text{acac})(\mathbf{1}-\mathbf{2})]^+$  compared to  $[\text{Cu}(\text{acac})(\mathbf{3}-\mathbf{4})]^+$ . The ENDOR spectra revealed a small variation in  $^1\text{H}$  (imine) and  $^{14}\text{N}$  spin densities as a function of the diimine ligand. The largest component of imine hyperfine couplings decreased as the ligand size increased, in the order of bipy > phen > Py-bipy > dppz, and concomitantly the largest component of the  $^{14}\text{N}$  hyperfine decreased according to the same trend in ligand size, owing to the greater spin delocalisation. These results indicate how even small structural and electronic (spin density) perturbations to the Casiopeina family of  $\text{Cu}(\text{II})$  complexes can be interrogated and probed by advanced EPR methods.

#### Declaration of Competing Interest

The authors declare that they have no known competing financial interests or personal relationships that could have appeared to influence the work reported in this paper. The dataset file associated with this work can be viewed at <http://doi.org/10.17035/d.2020.011271657>.

#### Acknowledgments

The authors would like to thank the EPSRC for financial support (EP/P019951).

#### References

- [1] C. Santini, M. Pelli, V. Gandin, M. Porchia, F. Tisato, C. Marzano, *Chem. Rev.* 114 (2014) 815–862.
- [2] M.E. Bravo-Gómez, J.C. García-Ramos, I. Gracia-Mora, L. Ruiz-Azuara, *J. Inorg. Biochem.* 103 (2009) 299–309.

- [3] L. Becco, A. Rodríguez, M.E. Bravo, M.J. Prieto, L. Ruiz-Azuara, B. Garat, V. Moreno, D. Gambino, *J. Inorg. Biochem.* 109 (2012) 49–56.
- [4] A. De Vizcaya-Ruiz, A. Rivero-Muller, L. Ruiz-Ramirez, G.E.N. Kass, L.R. Kelland, R.M. Orr, M. Dobrota, *Toxicol. Vitro* 14 (2000) 1–5.
- [5] C. Trejo-Solís, G. Palencia, S. Zúñiga, A. Rodríguez-Ropon, L. Osorio-Rico, S.T. Luvia, I. Gracia-Mora, L. Marquez-Rosado, A. Sánchez, M.E. Moreno-García, A. Cruz, M.E. Bravo-Gómez, L. Ruiz-Ramírez, S. Rodríguez-Enriquez, *J. Sotelo, Neoplasia* 7 (2005) 563–574.
- [6] F. Carvallo-Chaigneau, C. Trejo-Solís, C. Gómez-Ruiz, E. Rodríguez-Aguilera, L. Macías-Rosales, E. Cortés-Barberena, C. Cedillo-Peláez, I. Gracia-Mora, L. Ruiz-Azuara, V. Madrid-Marina, F. Constantino-Casas, *Biometals* 21 (2008) 17–28.
- [7] A. Tovar-Tovar, L. Ruiz-Ramirez, A. Campero, A. Romerosa, R. Moreno-Esparza, M.J. Rosales-Hoz, *J. Inorg. Biochem.* 98 (2004) 1045–1053.
- [8] M. O'Connor, A. Kellett, M. McCann, G. Rosair, M. McNamara, O. Howe, B.S. Creaven, S. McClean, A. Foltyn-Arfa Kia, D. O'Shea, M. Devereux, *J. Med. Chem.* 55 (2012) 1957–1968.
- [9] M.E. Katsarou, E.K. Efthimiadou, G. Psoimas, A. Karaliota, D. Vourloumis, *J. Med. Chem.* 51 (2008) 470–478.
- [10] N.R. Aliaga-Alcalde, P. Marqués-Gallego, M. Kraaijkamp, C. Herranz-Lancho, H. den Dulk, H. Görner, O. Roubeau, S.J. Teat, T. Weyhermüller, J. Reedijk, *Inorg. Chem.* 49 (2010) 9655–9663.
- [11] P.P. Silva, W. Guerra, J.N. Silveira, A.M.D.C. Ferreira, T. Bortolotto, F.L. Fischer, H.N. Terenzi, A. Neves, E.C. Pereira-Maia, *Inorg. Chem.* 50 (2011) 6414–6424.
- [12] A.M. Madalan, M. Noltemeyer, M. Neculai, H.W. Roesky, M. Schmidtman, A. Müller, Y. Journaux, M. Andruh, *Inorg. Chim. Acta* 359 (2006) 459–467.
- [13] J. Serment-Guerrero, P. Cano-Sanchez, E. Reyes-Perez, F. Velazquez-Garcia, M. E. Bravo-Gomez, L. Ruiz-Azuara, *Toxicol. Vitro* 25 (2011) 1376–1384.
- [14] A. De Vizcaya-Ruiz, A. Rivero-Müller, L. Ruiz-Ramirez, J.A. Howarth, M. Dobrota, *Toxicology* 194 (2003) 103–113.
- [15] C.H. Ng, S.M. Kong, Y.L. Tiong, M.J. Maah, N. Sukram, M. Ahmad, A.S.B. Khoo, *Metallomics* 6 (2014) 892–906.
- [16] M. Wehbe, A.W.Y. Leung, M.J. Abrams, C. Orvig, M.B. Bally, *Dalton Trans.* 46 (2017) 10758–10773.
- [17] T.F.S. Silva, L.M.D.R.S. Martins, *Molecules* (2020) 748.
- [18] M.C. Ryan, L.D. Whitmire, S.D. McCann, S.S. Stahl, *Inorg. Chem.* 58 (2019) 10194–10200.
- [19] J.E. Steves, S.S. Stahl, *J. Am. Chem. Soc.* 135 (2013) 15742–15745.
- [20] H. Lee, X. Wu, L. Sun, *Nanoscale* 12 (2020) 4187–4218.
- [21] T. Zhang, C. Wang, S. Liu, J.-L. Wang, W. Lin, *J. Am. Chem. Soc.* 136 (2014) 273–281.
- [22] S.M. Barnett, K.I. Goldberg, J.M. Mayer, *Nature Chem.* 4 (2012) 498–502.
- [23] J.D. Cope, H.U. Valle, R.S. Hall, K.M. Riley, E. Goel, S. Biswas, M.P. Hendrich, D.O. Wipf, S.L. Stokes, J.P. Emerson, *Eur. J. Inorg. Chem.* 14 (2020) 1278–1285.
- [24] X. Zeng, W. Yan, M. Paeth, S.B. Zacate, P.-H. Hong, Y. Wang, D. Yang, K. Yang, T. Yan, C. Song, Z. Cao, M.-J. Cheng, W. Liu, *J. Am. Chem. Soc.* 141 (2019) 19941–19949.
- [25] Y. Liu, H. Wang, J.-P. Wan, *J. Org. Chem.* 79 (2014) 10599–10604.
- [26] M. Chikira, Y. Tomizawa, D. Fukita, T. Sugizaki, N. Sugawara, T. Yamazaki, A. Sasano, H. Shindo, M. Palaniandavar, W.E. Antholine, *J. Inorg. Biochem.* 89 (2002) 163–173.
- [27] R. Galindo-Murillo, J. Hernandez-Lima, M. Gonzalez-Rendon, F. Cortes-Guzman, L. Ruiz-Azuara, R. Moreno-Esparza, *Phys. Chem. Chem. Phys.* 13 (2011) 14510–14515.
- [28] T. Hirohama, Y. Kuranuki, E. Ebina, T. Sugizaki, H. Arai, M. Chikira, P. Tamil Selvi, M. Palaniandavar, *J. Inorg. Biochem.* 99 (2005) 1205–1219.
- [29] R. Galindo-Murillo, L. Ruiz-Azuara, R. Moreno-Esparza, F. Cortes-Guzman, *Phys. Chem. Chem. Phys.* 14 (2012) 15539–15546.
- [30] R. Alemón-Medina, J.L. Muñoz-Sánchez, L. Ruiz-Azuara, I. Gracia-Mora, *Toxicol. Vitro* 22 (2008) 710–715.
- [31] J.-I. Ueda, M. Takai, Y. Shimazu, T. Ozawa, *Arch. Biochem. Biophys.* 357 (1998) 231–239.
- [32] A. Rivero-Müller, A. De Vizcaya-Ruiz, N. Plant, L. Ruiz, M. Dobrota, *Chem.-Biol. Interact.* 165 (2007) 189–199.
- [33] R. Alemón-Medina, M. Breña-Valle, J. Muñoz-Sánchez, M. Gracia-Mora, L. Ruiz-Azuara, *Cancer Chemother Pharmacol* 60 (2007) 219–228.
- [34] A. Eastman, *Biochemistry*, 25 (1986) 3912–3915.
- [35] A.M.J. Fichtinger-Schepman, J.L. Van der Veer, J.H.J. Den Hartog, P.H.M. Lohman, J. Reedijk, *Biochemistry* 24 (1985) 707–713.
- [36] E.R. Jamieson, S.J. Lippard, *Chem Rev* 99 (1999) 2467–2498.
- [37] B.M. Hoffman, *Proc. Natl. Acad. Sci. USA* 100 (2003) 3575–3578.
- [38] B.M. Hoffman, *Acc. Chem. Res.* 24 (1991) 164–170.
- [39] B.M. Hoffman, *Acc. Chem. Res.* 36 (2003) 522–529.
- [40] M. Chikira, C. Hee Ng, M. Palaniandavar, *Int. J. Mol. Sci.* 16 (2015) 22754–22780.
- [41] J.C. García-Ramos, R. Galindo-Murillo, A. Tovar-Tovar, A.L. Alonso-Saenz, V. Gómez-Vidales, M. Flores-Iamo, L. Ortiz-Frade, F. Cortes-Guzman, R. Moreno-Esparza, A. Campero, L. Ruiz-Azuara, *Chem. Eur. J.* 20 (2014) 13730–13741.
- [42] O.O.E. Onawumi, O.O.P. Faboya, O.A. Odunola, T.K. Prasad, M.V. Rajasekharan, *Polyhedron* 27 (2008) 113–117.
- [43] Y. Zhao, D.G. Truhlar, *Theor. Chem. Acc.* 120 (2008) 215–224.
- [44] F. Weigend, R. Ahlrichs, *Phys. Chem. Chem. Phys.* 7 (2005) 3297–3305.
- [45] C. Adamo, V. Barone, *J. Chem. Phys.* 110 (1999) 6158–6169.
- [46] V. Barone, in *Recent Advances in Density Functional Methods, Part 1* (ed. D. P. Chong), World Scientific, Singapore, 1995, 287.
- [47] S. Stoll, A. Schweiger, *J. Magn. Reson.* 178 (2006) 42–55.
- [48] A. Schweiger, *Struct. Bonding (Berlin)* 51 (1982) 1.
- [49] R. Miyamoto, Y. Ohba, M. Iwaizumi, *Inorg. Chem.* 31 (1992) 3138–3149.
- [50] S. Kita, M. Hashimoto, M. Iwaizumi, *Inorg. Chem.* 18 (1979) 3432–3438.
- [51] T.G. Brown, B.M. Hoffman, *Mol. Phys.* 39 (1980) 1073–1109.
- [52] M.E. Owen, E. Carter, G.J. Hutchings, B.D. Ward, D.M. Murphy, *Dalton Trans.* 41 (2012) 11085–11092.
- [53] A. Schweiger, H.H. Günthard, *Chem. Phys.* 32 (1978) 35–61.
- [54] D.M. Murphy, I. Caretti, E. Carter, I.A. Fallis, M.C. Göbel, J. Landon, S. Van Doorslaer, D.J. Willock, *Inorg. Chem.* 50 (2011) 6944–6955.
- [55] A. Schweiger, G. Rist, H.H. Günthard, *Chem. Phys. Lett.* 31 (1975) 48–52.
- [56] M.R. Healy, E. Carter, I.A. Fallis, R.S. Forgan, R.J. Gordan, E. Kamenetzky, J.B. Love, C.A. Morrison, D.M. Murphy, P.A. Tasker, *Inorg. Chem.* 54 (2015) 8465–8473.
- [57] G.H. Rist, J.S. Hyde, *J. Chem. Phys.* 52 (1970) 4633–4643.
- [58] B.M. Hoffman, J. Martinsen, J. Venters, *J. Magn. Reson.* 59 (1984) 110–123.
- [59] B.M. Hoffman, J. Venters, J. Martinsen, *J. Magn. Reson.* 62 (1985) 537–542.
- [60] G.C. Hurst, T.A. Henderson, R.W. Kreilick, *J. Am. Chem. Soc.* 107 (1985) 7294–7299.
- [61] T.A. Henderson, G.C. Hurst, R.W. Kreilick, *J. Am. Chem. Soc.* 107 (1985) 7299–7303.
- [62] D.M. Murphy, R.D. Farley, *Chem. Soc. Rev.* 35 (2006) 249–268.
- [63] K.M. Sharples, E. Carter, C.E. Hughes, K.D.M. Harris, J.A. Platts, D.M. Murphy, *Phys. Chem. Chem. Phys.* 15 (2013) 15214–15222.